SPACE WEATHER, VOL. 5, S11004, doi:10.1029/, 2007

Metrics analysis of the coupled Block Adaptive-Tree Solar Wind Roe-Type Upwind Scheme and Fok ring current model performance

A. Taktakishvili,[1] M. Kuznetsova,[1] M. Hesse,[1] L. Rastätter,[1] A. Chulaki,[1] and A. Pulkkinen[1]

Received 6 February 2007; revised 16 June 2007; accepted 1 August 2007; published 28 November 2007.

[1] Modeling is an important tool in understanding physical processes in the solar system. Metrics analysis evaluates model performance by comparing model output to a measurable parameter of interest. In this paper we studied the performance of the coupled Block Adaptive-Tree Solar Wind Roe-Type Upwind Scheme (BATSRUS) global magnetosphere MHD code and the Fok ring current model (FRC) by examining in detail the geosynchronous proton fluxes during the injection event on 21–22 January 2005. The output of BATSRUS code, calculated ionospheric potential and magnetic field, as well as proton temperature and density distribution, is used as an input boundary condition for the FRC model. We also discuss another event, on 10–11 August 2000, and speculate about the reasons of an apparent difference in the performance of the coupled models for these two events. The results of the simulation are compared with two LANL satellite observations, LANL-97A and 1994-084. The comparison of the simulation results for strongly varying solar wind and for prolonged interval of steady solar wind with southward IMF B_z, demonstrates that coupled BATSRUS and FRC models perform fairly for the magnetosphere driven by strong solar wind disturbances and probably are missing some internal magnetosphere dynamics in the second case.

Citation: Taktakishvili, A., M. Kuznetsova, M. Hesse, L. Rastätter, A. Chulaki, and A. Pulkkinen (2007), Metrics analysis of the coupled Block Adaptive-Tree Solar Wind Roe-Type Upwind Scheme and Fok ring current model performance, *Space Weather*, *5*, S11004, doi:10.1029/2007SW000321.

1. Introduction

[2] Scientific models are important tools in understanding physical processes in the solar system. They often provide a global view of a studied object that is not available using only satellite or ground observations and help to put observations into global context. Models are used by space weather operators for their applications and space weather forecasting. Therefore it is essential that the scientific community, operational users, and model developers are aware of model capabilities and limitations. One of the ways of measuring model effectiveness is the metrics analysis, standardized, repeatable comparison of model output to a measurable parameter of interest. The result is expressed as a skill score, a simple number, which measures the performance of a model against some reference model, based on modeling of one particular output parameter. Such studies provide continuous feedback to the model developers and encourage further modeling improvement. Metrics analysis is setting a benchmark for the current state of a model and thus is a tool for tracing model progress over time. It also gives information about the usefulness of a model upgrade. By having a simple single number like a skill score to characterize a model, it is easy to compare the performance of different models with similar output. Finally, metrics studies provide information about the usefulness of a model for operations and thus are of particular importance to space weather operators.

[3] In this paper we studied the performance of the coupled Block Adaptive-Tree Solar Wind Roe-Type Upwind Scheme (BATSRUS) global MHD code and the Fok ring current model (FRC). The results of the simulation are compared with the LANL-97A and 1994-084 geosynchronous satellite observations of energetic proton fluxes and a metrics analysis is performed.

[4] The Earth's ring current is a large-scale electric current system encircling Earth's magnetic equator at

[1]NASA Goddard Space Flight Center, Greenbelt, Maryland, USA.

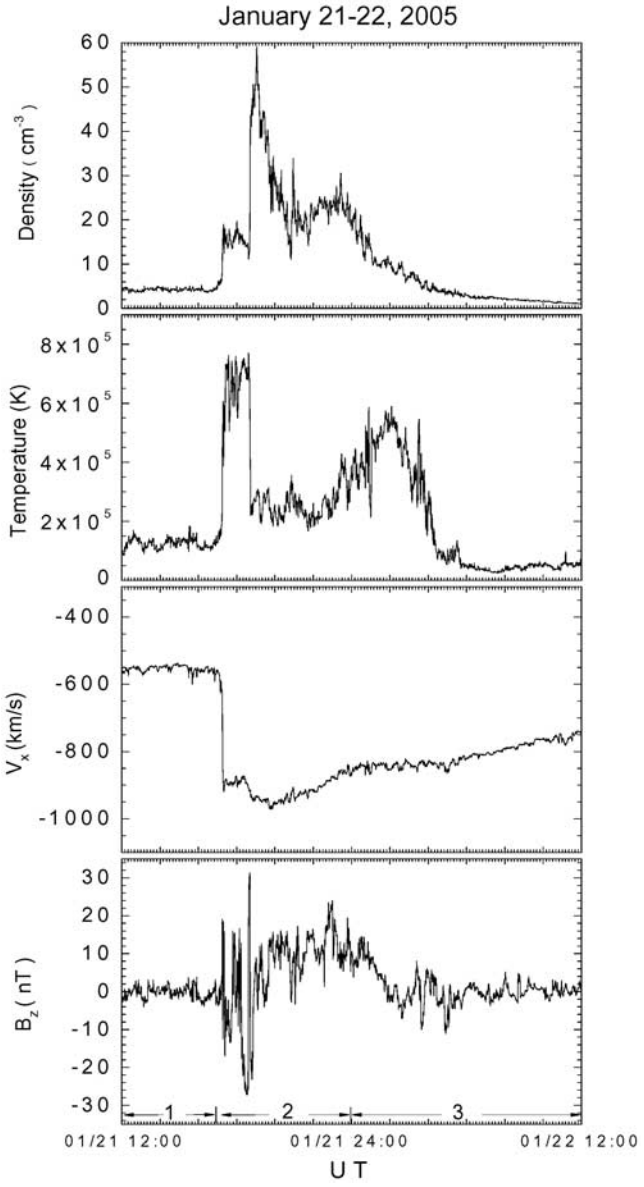

Figure 1. ACE satellite solar wind data for the 21–22 January 2005 event.

radial distances typically in the range from 2 to 8 R_E [e.g., *Fok et al.*, 2001]. The current is carried mainly by westward drifting trapped 1–300 keV ions [*Daglis et al.*, 1999] injected from the inner plasma sheet through the nightside geosynchronous orbit region [*Wolf et al.*, 1997; *Fok et al.*, 1996]. Geosynchronous orbit injections of charged particles and the ring current buildup are the subject of intensive studies using both observations and modeling due to the importance of this region of the inner magnetosphere for theoretical and practical purposes.

[5] One of the most popular and frequently applied models of the ring current is the Fok ring current model (FRC) [*Fok et al.*, 1995, 1999; *Fok and Moore*, 1997]. At the Community Coordinated Modeling Center at NASA/GSFC, Fok rung current model is coupled with the global magnetosphere MHD code BATSRUS [*Powell et al.*, 1999], which is used as a driver for the ring current model.

[6] In this study we perform detailed metrics analysis of the coupled BATSRUS and FRC model performance for the geosynchronous proton injection event on 21–22 January 2005. We also demonstrate the limitations of the model capabilities using another proton injection event on 10–11 August 2000.

2. Brief Description of BATSRUS and Fok Rig Current Models and Solar Wind Input Conditions

[7] The University of Michigan global MHD magnetosphere model BATSRUS [*Powell et al.*, 1999] uses solar wind input as an upstream boundary condition. It calculates, self-consistently, the magnetic field, ionospheric potential, and plasma sheet temperature and density distribution. These parameters are then used as input to the FRC model.

[8] The Fok ring current model (FRC) calculates the differential particle fluxes for protons and electrons up to 300 keV by solving a bounce-averaged Boltzmann transport equation for a phase space distribution function along magnetic field lines. The phase space distribution is assumed to be constant along magnetic field lines at constant first and second invariant for an arbitrary pitch angle distribution. The advection terms include gradient-curvature drift and $\mathbf{E} \times \mathbf{B}$ drift, which includes both corotation and the convection. In addition, the model calculates losses due to charge exchange. The initial source population uses the quiet time ion composition compiled by *Sheldon and Hamilton* [1993], which was obtained using the Active Magnetospheric Particle Tracer Explorer/Charge Composition Explorer/Charge-Energy-Mass instrument. The outer boundary of the FRC model is at 10 R_E on the nightside and at the last closed field line on the dayside magnetosphere. After the initial setup, temperature and density of protons at the outer boundary, and ionospheric potential and magnetic field given by MHD code BATSRUS are used as input to the FRC model. The pitch-angle distribution on the boundary is assumed to be isotropic.

[9] The solar wind input to the BATSRUS code in the studied event is presented in Figure 1. It is given for the interval 21 January, 1200 UT to 22 January, 1200 UT and corresponds to ACE satellite data projected to the distance of 33 R_E (GSM), which is the boundary of the BATSRUS model. The projection is performed by averaging the solar wind velocity at the ACE location (L1 point) and assuming the signal propagation from L1 to 33 R_E with this average velocity. It is clear from this plot that all solar wind parameters exhibit a sharp jump at approximately

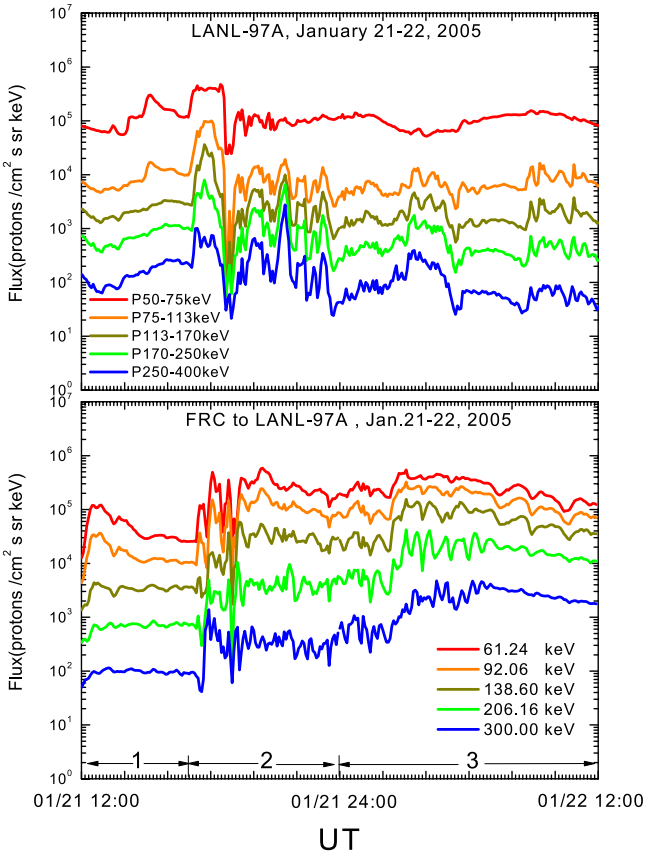

Figure 2. LANL-97A geosynchronous satellite proton flux data and the Fok ring current model results mapped to this satellite trajectory.

21 January, 1700 UT. We will show below how this abrupt change reflects geosynchronous particle luxes.

3. Observation and Simulation Results

[10] The results of observations and the model calculations are shown in Figure 2. Figure 2a shows LANL-97A geosynchronous satellite SOPA instrument proton fluxes [see, e.g., *Reedy et al.*, 1998] color-coded for four energy channels: P2, 75–113 keV (red); P3, 113–170 keV (orange); P4, 170–250 keV (green); and P5, 250–400 keV (blue). We do not consider the lowest energy proton channel P1, 50–75 keV, in this paper because for P1 electronic noise contaminates the real proton counts for the studied event (G. Reeves, private communication, 2006). Figure 2b shows the FRC simulation results mapped to the satellite trajectory. Proton fluxes are calculated from FRC model for energies correspondent to the geometric mean of the minimum and maximum energies of the four energy channels.

[11] Fluxes on both Figures 2a and 2b exhibit a sharp increase very quickly after 21 January, 1700 in correspondence to sharp changes of solar wind conditions at this moment of time (Figure 1). This indicates that solar wind is a direct driver of the ring current variations during the 21–22 January 2005 event. The time series of fluxes look quite similar in both Figures 2a and 2b, so the coupled models do a fair job qualitatively. The quantitative metrics analysis of the model performance is presented in the next two sections. First, we perform a more traditional, correlation based metrics analysis. After that we show the results of an event prediction based metrics analysis, which we think is more relevant in the considered case.

4. Correlation Based Metrics

[12] In order to perform correlation based metrics analysis we divide the whole 24-h time interval into three subintervals according to the flux behavior in Figure 2: (1) 21 January, 1200, to 21 January, 1700, prestorm quiet interval; (2) 21 January, 1700, to 21 January, 2400, active interval (the sharp jump in fluxes is included in this interval); (3) 21 January 2400 to 22 January 1200 post-active interval. We estimate model performance for these three intervals separately as well as for the whole interval.

[13] For the correlation based metrics analysis we use the concepts of a reference model, model score, and skill score. A reference model is a model to which both simulation results and measurements are compared to for a needed parameter. In our case this parameter is proton flux F. We consider two different reference models in our analysis: the mean model and the persistence model. For the mean model no perturbations are assumed. It is characterized by a single number F_{mean} equal to the mean value of the measured flux $\langle F_{obs}(t)\rangle$ for the considered time interval. The persistence model uses previous measurements as a prediction. For example, for 5 min period persistence, flux $F_{pers}(t)$ at a given moment of time t is equal to the flux observed 5 min earlier, F_{obs}(t–5 min). The smaller the persistence period, the closer the persistence model is to the observations.

[14] A model score D is a standard deviation of the difference between the model results and the measurements. With the fluxes $F_{m,r}$ and F_o given by the simulation model (or the reference model) and the observations, respectively, the score for the simulation (or the reference) model, $D_{m,r}$ is calculated by:

$$D_{m,r} = \sqrt{\frac{\sum |F_{m,r} - F_o|^2}{N_{\text{points}}}} \qquad (1)$$

where N_{points} is the number of points in the observations.

[15] After introducing the model score we can now introduce a single number which characterizes the model performance versus the reference model for a given interval of time as:

$$M = 1 - \frac{D_m}{D_r} \qquad (2)$$

M is called a skill score and its value indicates how well the model performs in respect to the reference model: (1) $M = 0$ -the model performance is as good as performance of the reference model; (2) $M < 0$ -performance is worse; (3) $0 < M < 1$ -performance is better; (4) $M = 1$ -performance is perfect.

[16] Figures 3 and 4 show the calculated skill scores for the model in respect to the mean model (black squares), 25 min persistence model (blue triangles), 50 min persistence model (green triangles), and 100 min persistence model (red circles) versus an energy channel number. In Figures 3a and 3c and Figures 4a and 4c the skill scores for proton flux F are presented; Figures 3b and 3d and Figures 4b and 4d demonstrate skill scores for $\log_{10}$(F), that is, for the order of magnitude of the flux. Figures 3a and 3b correspond to first, prestorm quiet time interval Figures 3c and 3d correspond to the second, active interval. Figures 4a and 4b correspond to third, postactive interval and Figures 4c and 4d correspond to the whole time interval.

[17] Figures 3 and 4 show that the behavior of the skill score versus energy is qualitatively similar in respect to all reference models, mean, or persistence, but it depends on the considered time interval: (1) M has a maximum for the fourth energy channel for the prestorm, quiet interval; (2) M monotonically grows with energy for the active interval; (3) M has a minimum for the third channel for the postactive interval and also for the whole interval. Not surprisingly, the skill score with respect to persistence model is higher for larger persistence period.

[18] There is an energy-dependence of the skill for all models. Excluding channel P2 the model performs better than the mean reference model for the prestorm quiet interval (see all energies). For 50 and 100 min persistence periods the relative performance of the model for the two intervals depends on energy. The skill score for the third, postactive period is extremely low, and this influences the result for the whole interval (see Figure 4). The performance of the model with respect to the order of magnitude of the flux ($\log_{10}$(F)) is much better (compare left and right columns in Figures 3 and 4).

5. Event Prediction-Based Metrics

[19] Correlation-based analysis is not always the best way to evaluate model performance. This is especially true for the complex form of the measured quantity behavior in time. Besides, correlation based metrics often lacks user relevance. In many cases a metrics based on some overall aspect of the measured quantity, like the amplitude, should be preferred. This can help in the actual decision process involving the forecast-mitigation action. Both of these reasons are valid in our case. First, the geosynchronous orbit proton flux time variation is rather complex. Second, rather than knowing skill score, more informative would be, for example, to know how well coupled BATSRUS and FRC models predict for the proton flux exceeding of certain threshold level $F_m > F_{thr}$.

[20] Metrics analysis based on a study of model capability to predict ''events'' was suggested and used by *Weigel et al.* [2006] and used, for example, by *Pulkkinen et al.* [2007]. It was introduced to characterize the utility of the model: what would be the monetary gain/loss if the system mitigates according to the model predictions. The utility is compared with respect to a reference system that is never mitigated.

[21] In our case an ''event'' can be defined as follows: within a forecast window of length ΔT_{win}, proton flux exceeds a threshold F_{thr}. The window is moved over the entire time interval in such a way that analyzed parts of the time series do not overlap. The forecast is correct if both the model and measurement exceed F_{thr} at least once within a window. A false alarm happens if within a window the model predicts $F_m > F_{thr}$, while the measured flux never exceeds the threshold value. Since in the ''event'' prediction-based metrics, the utility is compared with respect to a reference system that is never mitigated, it is not necessary to include misses, that is, failure of the model to predict the flux exceeding some threshold, since such misses do not influence monetary gain/loss (see *Weigel et al.* [2006] and *Pulkkinen et al.* [2007] for the details).

[22] All correct and false predictions within each window are summed then for the entire time interval to obtain a number of correct N_{cr} and false N_{fs} predictions. Metrics based on ''event'' prediction is characterized by the ratio $R_f = N_{cr}/N_{fs}$, called the forecast ratio.

[23] The results of the event prediction-based metrics analysis for the coupled models and LANL-097A satellite measurements are presented in Figure 5. In this case we consider the whole 24 h period of the observations, correspondent to 21 January, 1200 UT to 22 January, 1200 UT. In Figures 5a and 5b the forecast ratio versus threshold level F_{thr} is shown. Figure 5a corresponds to the lowest considered energy channel P2 (75−113 keV). The forecast ratio for three different window lengths, 60 min, 30 min, and 15 min is demonstrated in Figure 5a. The lower panel shows the same for the highest energy channel P5 (250 keV-400 keV). For each channel we took the appropriate threshold range.

[24] As we can see, coupled models give more correct predictions than false alarms (R_f) for lower threshold values for both channels. Then, the forecast ratio is dropping for growing threshold levels. For a given F_{thr}, R_f is larger for larger window lengths. Comparing Figures 5a and 5b for the same window length indicates that the model works slightly better for the higher-energy channel, although we have to remember that forecast ratios are calculated for different threshold levels for two different energy channels.

[25] In Figure 6 we show the forecast ratio versus F_{thr} for a different persistence and fixed window length ΔT_{win} = 30 min. We plot in Figures 6a and 6b also the

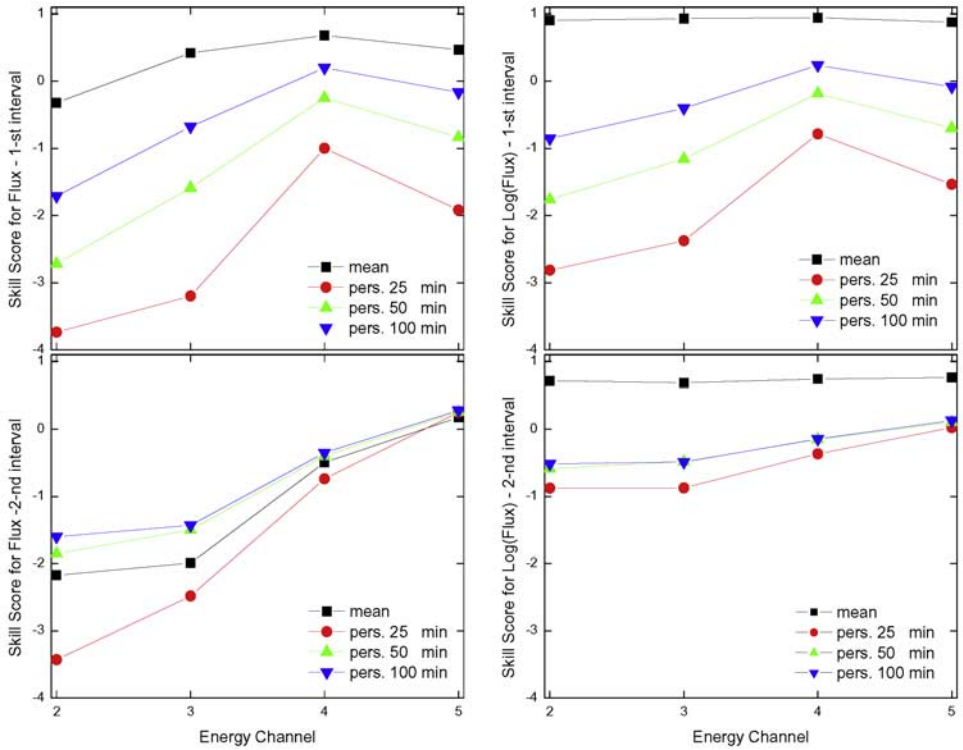

Figure 3. The model performance skill score versus energy channel number for the first (prestorm quiet) and the second (active) time intervals.

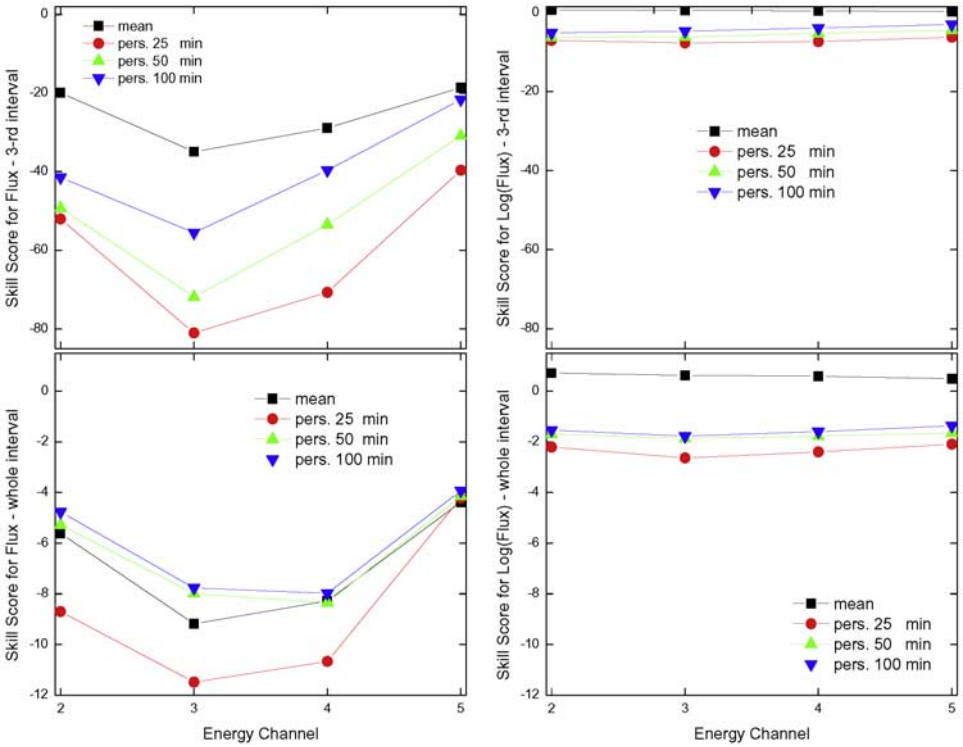

Figure 4. The model performance skill score versus energy channel number for the third (postactive) and the whole intervals.

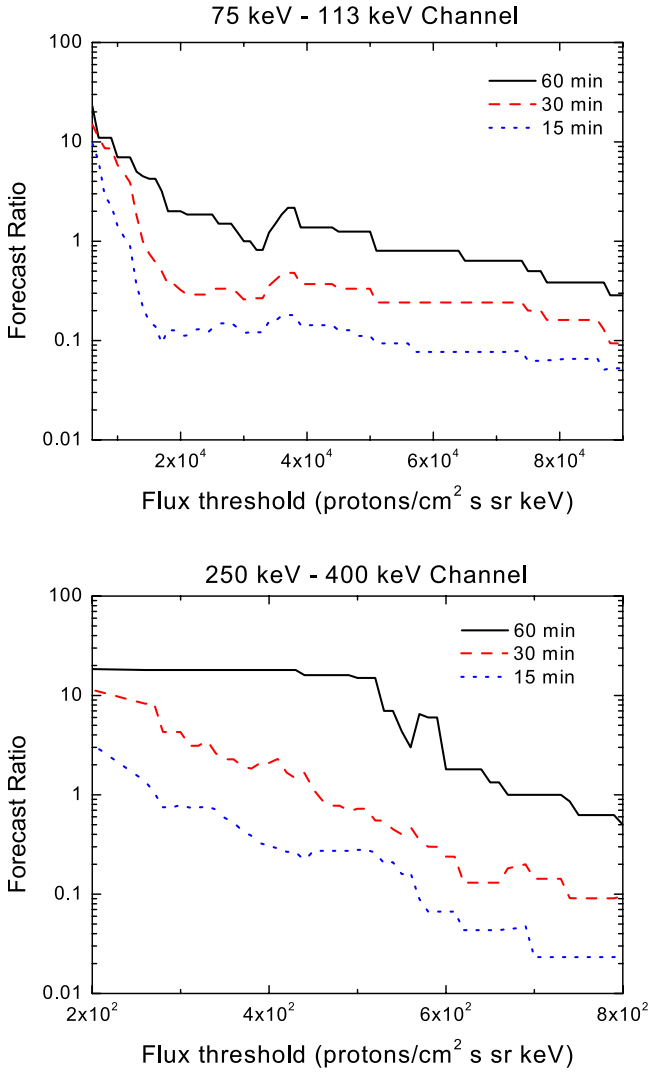

Figure 5. The orecast ratio versus flux threshold level for different forecast window lengths, showing (a) energy channel 50–75 keV and (b) energy channel 250–400 keV.

corresponding forecast ratio for the model for the same window length. We see that the coupled models perform worse than persistence. The difference in performance is somewhat smaller for the higher-energy channel.

6. Limitations of the Model: Event of 10–11 August 2000

[26] The limitations of the coupled BATSRUS and FRC models can be clearly seen from the analysis of model performance for another event, a so-called "sawtooth" profile proton injection event on 10–11August 2000, studied in detail by *Henderson et al.* [2006]. "Sawtooth" injections are called quasi-periodic, large-amplitude oscillations of energetic particle fluxes at the geosynchronous orbit during prolonged intervals of steady southward IMF B_z [e.g., *Reeves et al.*, 2004]. In order to illustrate more clearly the difference between the 10–11 August 2000 event and the event on 21–22 January 2005, analyzed in previous sections, in Figure 7 we placed the observation and model results for these two events next to each other. The left column represents the 21–22 January 2005 event and the right column represents the 10–11 August 2000 event. Figures 7a–7d represent corresponding solar wind data. Therefore Figures 7a–7d repeat Figure 1 in the left column. Figures 7e and 7f show observation data and model calculation results for geosynchronous proton fluxes, so they repeat Figure 2 in the left column.

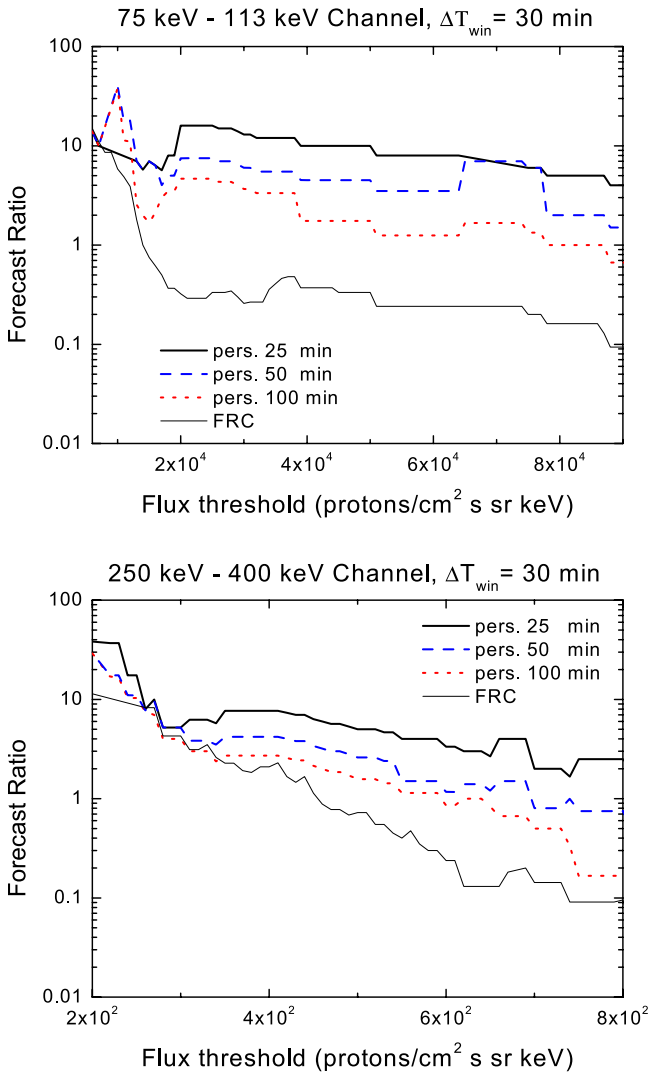

Figure 6. Forecast ratio versus flux threshold level for 30 min window length and different persistence models, showing (a) energy channel 50–75 keV and (b) energy channel 250–400 keV.

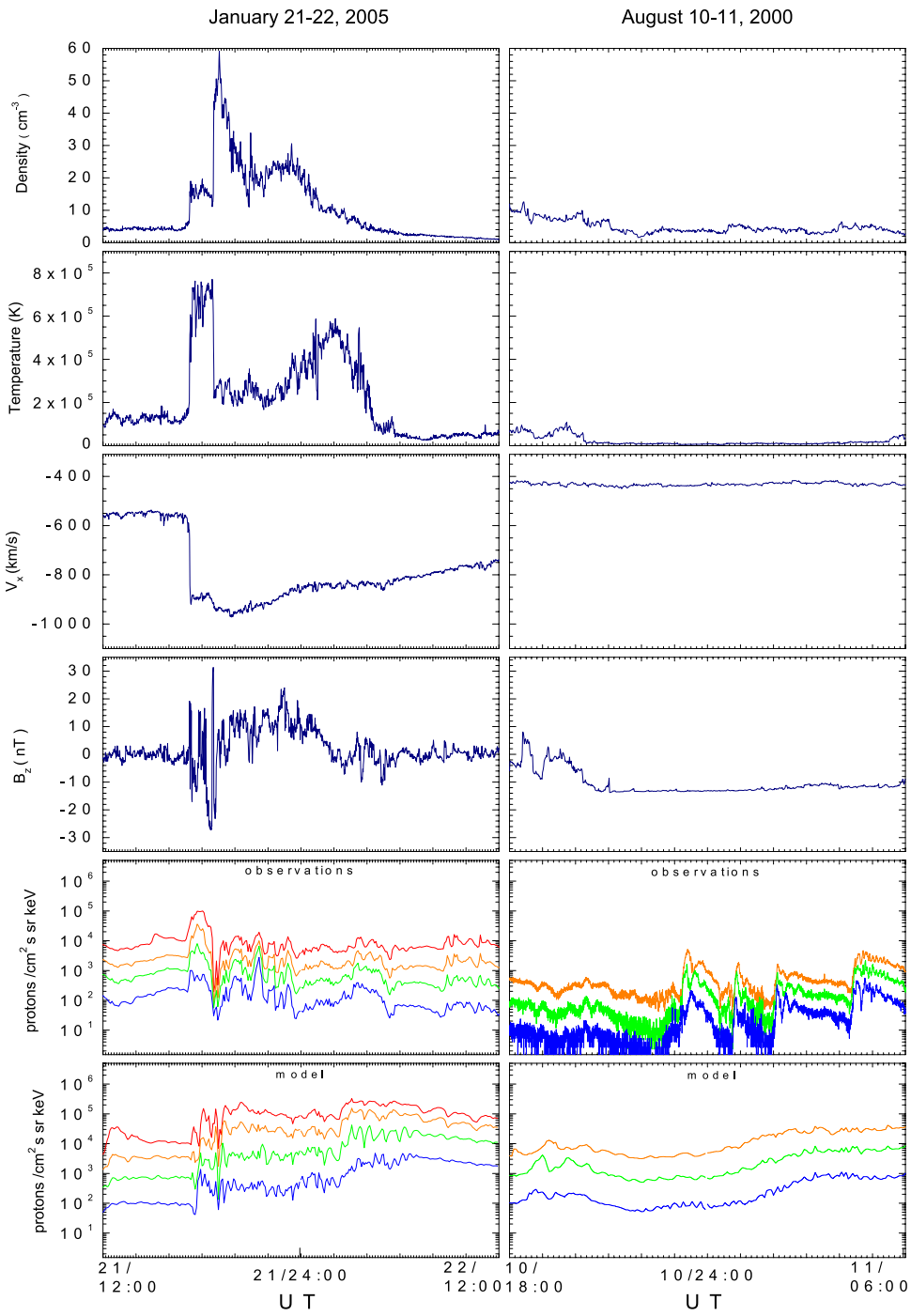

Figure 7. Comparison of observation and model results for the (left) 21–22 January 2005 and (right) 10–11 August 2000 proton injection events, representing (a–d) corresponding solar wind data and (e–f) observation data and the model calculations for geosynchronous proton fluxes.

[27] In Figures 7e and 7f in the right column we show fluxes for three higher-energy proton channels, P3, P4, and P5, since lower-energy channels P1 and P2 were strongly contaminated by electronic noise for the 10–11 August 2000 event (G. Reeves, private communication, 2006).

[28] As we see, unlike the 21–22 January 2005 event, there is not even a resemblance between observations and

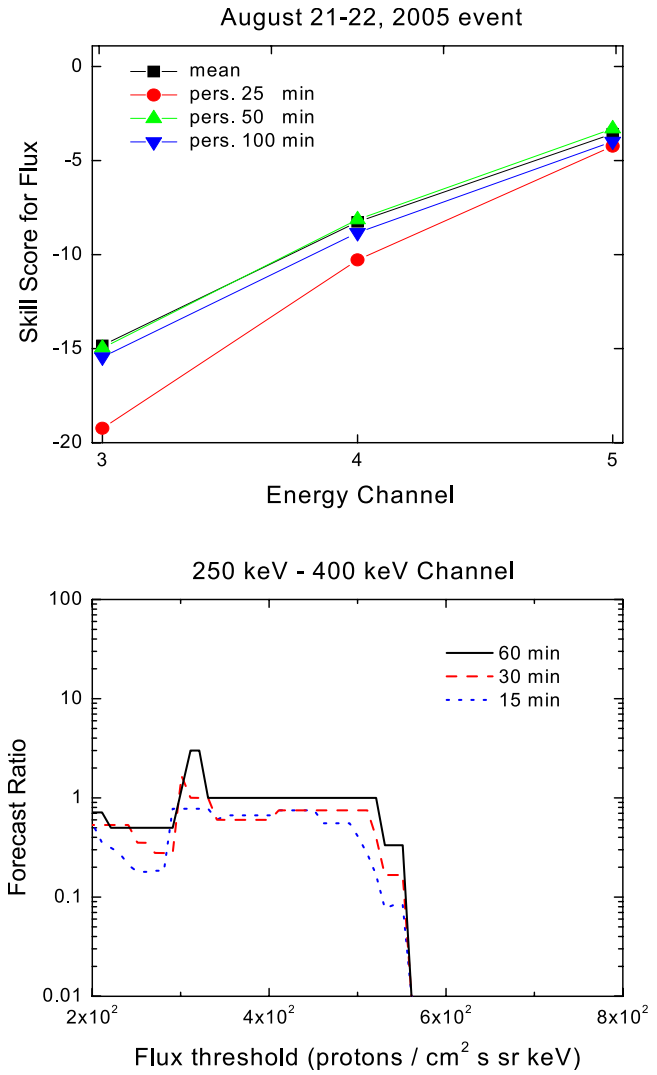

Figure 8. (a) Results of the correlation and (b) the event-based metrics calculations for the 21–22 August 2000 event. Figure 8a shows the model performance skill score with respect to the mean and the persistence reference models versus energy channel number. Figure 8b shows the forecast ratio versus flux threshold level for the different forecast window lengths for the energy channel 250–400 keV.

model calculations for the 10–11 August 2000 event. In Figure 8 we present the results of the metrics calculations for this event based on the whole interval of observations. Figure 8a demonstrates the result of the correlation metrics analysis: shown is skill score of the model performance with respect to the mean and the persistence reference models for different energy channels. Figure 8b demonstrates the result of event-based metrics analysis: shown is the forecast ratio for the highest-energy channel for different window lengths as a function of flux threshold level for correspondent flux interval.

[29] Comparing Figure 8a with Figure 3, we conclude that the skill score of the model performance for the 10–11 August 2000 event as a whole is lower than the skill score for the first and the second intervals of the 21–22 January 2005 event. However, it is higher than the extremely low skill score for the third interval of the 21–22 January 2005 event (see Figure 4). The comparison with the whole interval of the 21–22 January 2005 event shows that the skill score for the 10–11 August 2000 event is lower for the P3 energy channel and is almost the same for both events for P4 and P5.

[30] A better indication of the relative model performance appears to be given by event-based metrics analysis, characterized by the forecast ratio. Comparison of the Figure 8b with Figure 5b, showing the forecast ratio for the 21–22 January 2005 event for the same energy channel, demonstrates that the coupled model performance for the 10–11 August 2000 event is much worse.

[31] We would like to speculate about the possible reasons for such a discrepancy in model performance. Comparing solar wind data for these two events, one can clearly see that for 21–22 January 2005 the magnetosphere seems to be directly driven by strong, stormy solar wind disturbances, including strong IMF B_z component oscillations, which we believe cause geosynchronous flux oscillations. In this case the coupled models catch the basic features of the event, so we can say that their performance is satisfactory. On the other hand, on 10–11 August 2000 the solar wind is almost steady starting at 2100 UT and the IMF B_z component is quasi constant, directing southward. However, geosynchronous fluxes still exhibit rather strong "sawtooth" profile oscillations. In this case magnetosphere dynamics seems to be determined by some internal mechanism which the coupled models are apparently missing.

[32] We believe that the reason is in unphysical numerical resistivity, used in MHD codes, which allows to respond to the variations in the solar wind but produces a steady magnetosphere for steady solar wind conditions. Recently, *Kuznetsova et al.* [2007] used the BATSRUS model to analyze the influence of different dissipation mechanisms triggering magnetic reconnection, including nongyrotropic effects, in the magnetotail region.

[33] By introducing kinetic corrections, the authors were able to reproduce fast magnetotail reconnection rates observed in kinetic simulations and obtained quasi-periodic loading unloading cycles (multiple reconnection) in the magnetotail even for steady southward IMF conditions. In the followed work [*Taktakishvili et al.*, 2007], we used the FRC model to investigate the buildup of the ring current during the magnetotail loading-unloading cycles in the course of the long period of steady southward IMF. As input to the FRC model, we used the results of the simulation employing the technique developed by *Kuznetsova et al.* [2007]. This coupled modeling allowed

us to reproduce, for the first time in theoretical simulations, the ''sawtooth'' oscillations in the ring current: quasi-periodic, large-amplitude oscillations of energetic particle fluxes at the geosynchronous orbit during prolonged intervals of negative IMF B_z. However, modeling with kinetic corrections to MHD code is still under development and presently can be used to simulate only idealized solar wind conditions, not real events. Since we are studying real events, in the presented paper we used BATSRUS code without kinetic corrections. That is why the coupled models did not reproduce observed ''sawtooth'' type oscillations for the 10–11 August 2000 event because the solar wind was rather steady in this case: we believe that ''sawtooth'' events are caused by multiple reconnection (multiple substorms) in the magnetotail, which the model, with numerical resistivity alone, can not reproduce. These considerations give us the ground to speculate about the 21–22 January 2005 event to be directly driven by the solar wind disturbances and the 10–11 August 2000 event to be the result of the internal tail dynamics.

7. Summary

[34] We studied the performance of the coupled global MHD code BATSRUS and the Fok ring current models. The results of the simulation of the proton fluxes F are compared with the LANL satellite observations of geosynchronous proton injections. In order to evaluate the model performance we used two different methods: correlation based metrics analysis and event prediction metrics analysis.

[35] The correlation based metrics analysis suggests that models perform better than the mean reference model almost for all energies for the prestorm quiet interval. Skill score for the postactive period is rather low. The performance of the model for the order of magnitude of the flux ($\log_{10}(F)$) is much better.

[36] Event prediction based metrics analysis shows that the model gives more correct predictions than false alarms for lower flux prediction threshold levels F_{thr}. Persistence performs better than the models for the considered persistence periods and energies. The model performance is slightly better for higher energies than for lower energies. So, quantitatively the persistence models are hard to beat, but coupled BATSRUS and FRC models give satisfactory prediction for the order of magnitude and the profile of geosynchronous proton flux time series.

[37] We compared the model performance for driven magnetosphere, during strongly varying solar wind, to the model performance during a prolonged interval of steady solar wind, with IMF B_z directed southward. This comparison demonstrates the capabilities and limitations of the coupled BATSRUS and FRC models, important for practical operational purposes. It shows that the coupled models perform fairly for the magnetosphere driven by strongly disturbed solar wind and certainly better than for the case, when for a prolonged interval of time, solar wind disturbances are weak and IMF Bz is directed southward. We argue that models are apparently missing some internal magnetosphere dynamics, in this second case.

[38] We also speculate about the possible reasons of such a discrepancy in model performance. Our conclusions are based on the results of a recent model improvement by *Kuznetsova et al.* [2007], where the authors considered kinetic corrections to the MHD model simulations using coupled BATSRUS and FRC models. With this approach it is possible to address events like the event on 10–11 August 2000, discussed in section 6. However, modeling considering kinetic corrections to MHD code is still under development and presently can be used to simulate only idealized solar wind conditions, not real events. Modeling of real events is the subject of future work.

[39] **Acknowledgments.** We wish to thank M.-C. Fok and D. Berrios for valuable comments and help. We wish also to thank G. Reeves for helping with LANL satellite data and important remarks. This work was performed while one of the authors (A. T.) held a NRC/ORAU Research Associateship Award at NASA Goddard Space Flight Center. Computations were performed at the Community Coordinated Modeling Center through the runs-on-request system.

References

Daglis, I. A., R. M. Thorne, W. Baumjohann, and S. Orsini (1999), The terrestrial ring current: Origin, formation, and decay, *Rev. Geophys.*, *37*, 407–438.

Fok, M.-C., and T. E. Moore (1997), Ring current modeling in a realistic magnetic field configuration, *Geophys. Res. Lett.*, *24*, 1775–1778.

Fok, M.-C., T. E. Moore, J. U. Kozyra, G. C. Ho, and D. C. Hamilton (1995), Three-dimensional ring current decay model, *J. Geophys. Res.*, *100*, 9619–9632.

Fok, M.-C., T. E. Moore, and M. E. Greenspan (1996), Ring current development during storm main phase, *J. Geophys. Res.*, *101*, 15,311–15,322.

Fok, M.-C., T. E. Moore, and D. C. Delcourt (1999), Modeling of inner plasma sheet and ring current during substorms, *J. Geophys. Res.*, *104*, 14,557–14,569.

Fok, M.-C., R. A. Wolf, R. W. Spiro, and T. E. Moore (2001), Comprehensive computational model of Earth's ring, *J. Geophys. Res.*, *106*, 8417–8421.

Henderson, M. G., et al. (2006), Substorms during the 10–11 August 2000 sawtooth event, *J. Geophys. Res.*, *111*, A06206, doi:10.1029/2005JA011366.

Kuznetsova, M. M., M. Hesse, L. Rastätter, A. Taktakishvili, G. Toth, D. L. De Zeeuw, A. Ridley, and T. I. Gombosi (2007), Multiscale modeling of magnetospheric reconnection, *J. Geophys. Res.*, *112*, A10210, doi:10.1029/2007JA012316.

Powell, K. G., P. L. Roe, T. J. Linde, T. I. Gombosi, and D. L. DeZeeuw (1999), A solution-adaptive upwind scheme for ideal magnetohydrodynamics, *J. Comput. Phys.*, *154*, 284–309.

Pulkkinen, A., M. Hesse, M. Kuznetsova, and L. Rastaetter (2007), First-principles modeling of geomagnetically induced electromagnetic fields and current from upstream solar wind to the surface of Earth, *Ann. Geophys.*, *25*, 881–891.

Reedy, R. C., R. D. Belian, T. E. Cyon, M. G. Henderson, J. C. Ingraham, J.-M. Jahn, P. S. McLachlan, M. M. Meier, G. D. Reeves, and L. A. Weiss (1998), Long-term energetic-particle databases from geosyn-

chroneous and GPS orbits, paper presented at Conference on the High-Energy Radiation Background in Space, 22–23 July 1997, Inst. of Electr. and Electron. Eng., New York.

Reeves, G. D., et al. (2004), IMAGE, POLAR, and geosynchronous observations of substorm and ring current ion injections, in *Disturbances in Geospace: The Storm Substorm Relationship*, *Geophys. Monogr. Ser.*, vol. *142*, edited by A. S. Sharma, Y. Kamide, and G. S. Lakhina, pp. 91–101, AGU, Washington, D.C.

Sheldon, R. B., and D. C. Hamilton (1993), Ion transport and loss in the Earth's quiet ring current: 1. Data and standard model, *J. Geophys. Res.*, *98*, 13,491–13,508.

Taktakishvili, A., M. Kuznetsova, M. Hesse, M.-C. Fok, L. Rastaetter, M. Maddox, A. Chulaki, T. Gombosi, and D. L. De Zeeuw (2007), Buildup of the ring current during periodic loading-unloading cycles in the magnetotail driven by steady southward IMF, *J. Geophys. Res.*, *112*, A09203, doi:10.1029/2007JA012317.

Weigel, R. S., T. Detman, E. J. Rigler, and D. N. Baker (2006), Decision theory and the analysis of rare event space weather forecasts, *Space Weather*, *4*, S05002, doi:10.1029/2005SW000157.

Wolf, R. A., J. W. Freeman Jr., B. A. Hausman, R. W. Spiro, R. V. Hilmer, and R. L. Lambour (1997), Modeling convection effects in magnetic storms, in *Magnetic Storms*, *Geophys. Monogr. Ser.*, vol. *98*, edited by B. T. Tsurutani et al., pp. 161–172, AGU, Washington, D. C.

A. Chulaki, M. Hesse, M. Kuznetsova, A. Pulkkinen, L. Rastätter, and A. Taktakishvili, NASA Goddard Space Flight Center, Greenbelt, MD 20771, USA. (staktak@helio.gsfc.nasa.gov)